ChemComm

COMMUNICATION

View Article Online
View Journal | View Issue

Cite this: *Chem. Commun.*, 2018, 54, 78

Received 18th September 2017,
Accepted 27th November 2017

DOI: 10.1039/c7cc07259g

rsc.li/chemcomm

Hierarchical $CuCo_2S_4$ nanoarrays for high-efficient and durable water oxidation electrocatalysis†

Lin Yang,[a] Lisi Xie,[a] Xiang Ren,[a] Ziqiang Wang,[a] Zhiang Liu,[b] Gu Du,[c] Abdullah M. Asiri,[d] Yadong Yao[e] and Xuping Sun*[a]

It is highly attractive to design and develop earth-abundant electrocatalysts toward high-efficiency water oxidation electrocatalysis in alkaline media. In this communication, we report the *in situ* hydrothermal sulfidization preparation of a hierarchical $CuCo_2S_4$ nanoarray on copper foam ($CuCo_2S_4$/CF) from its $CuCo_2$-hydroxide nanowire array precursor. When used as a 3D catalyst electrode for water oxidation, the as-prepared $CuCo_2S_4$/CF is superior in catalytic activity, demanding overpotentials of only 259 and 295 mV to achieve 60 and 100 mA cm^{-2} in 1.0 M KOH, respectively. Moreover, it also shows strong electrochemical durability with high turnover frequency values of 0.069 and 0.390 mol O_2 s^{-1} at overpotentials of 300 and 400 mV, respectively.

The drastic depletion of fossil fuels and growing global environmental concerns call for an urgent demand for exploiting eco-friendly and renewable energy carriers.[1,2] Clean and sustainable hydrogen is regarded as an ideal candidate to replace fossil fuels.[3,4] Water electrolysis provides us an attractive way to produce pure hydrogen on a large scale.[5,6] Involving a multi-electron transfer process, anodic water oxidation remains a bottleneck for water electrolysis, thus efficient water oxidation catalysts (WOCs) are required to accelerate the kinetics, for achieving high current densities at minimal overpotentials.[7–9] Although Ru- and Ir-based oxides show the highest catalytic activity toward water oxidation, their low abundance and high cost greatly hinder their widespread commercial uses.[10]

Tremendous efforts have been devoted to developing earth abundant WOCs for more energy-efficient water electrolysis.[11–22] Transition metal sulfides (TMSs) have been widely investigated for energy storage and catalysis, such as lithium ion batteries,[23–25] supercapacitors,[26–28] hydrodesulfurization,[29–31] and electrochemical water splitting.[32–40] For catalyzing water oxidation, bimetallic TMSs are more competitive than monometallic ones.[35,41–43] Among them, big-cell sulphospinels can expose a large number of edge sites, with more rapid electron transfer pathways, smaller optical band gaps, and better redox reactions, offering great benefits to enhance electrochemical performances.[38,44–46] Recent works demonstrated that nanoarray catalysts have obvious advantages of exposing more active sites and facilitating diffusion of electrolytes and evolved gas.[6,11,13,47,48] Moreover, nanoarray catalysts with hierarchical feature would offer more active sites and have attracted increasing attention.[48–51] Therefore, hierarchical structured transition metal sulphospinels hold great promise for electrochemical water oxidation.

Herein, we describe the fabrication of a hierarchical $CuCo_2S_4$ nanoarray on copper foam ($CuCo_2S_4$/CF) by hydrothermally sulfidizing its bimetallic hydroxide nanowire array precursor (see the ESI† for preparation details). The as-prepared $CuCo_2S_4$/CF exhibits superior activity for water oxidation, needing overpotentials of only 259 and 295 mV to achieve 60 and 100 mA cm^{-2} in 1.0 M KOH, respectively, outperforming monometallic cobalt sulphide on CF (Co–S/CF) and copper sulphide on CF (Cu–S/CF). Notably, this system also demonstrates strong long-term electrochemical durability with high turnover frequency (TOF) values of 0.069 and 0.390 mol O_2 s^{-1} at overpotentials of 300 and 400 mV, respectively.

Fig. 1a presents the X-ray diffraction (XRD) patterns for $CuCo_2S_4$/CF. The peaks at 26.6°, 31.3°, 38.0°, 47.0°, 50.0°, 55.0°, and 64.4° can be indexed to the (022), (113), (004), (224), (115), (044), and (335) planes of the cubic $CuCo_2S_4$ phase (JCPDS No. 42–1450),[52–54] respectively, and the three peaks at 43.3°, 50.4°, and 74.1° arise from the CF substrate (JCPDS No. 04–0836). Fig. S1a and S1b show the XRD patterns for Cu–S/CF and Co–S/CF, indexed to the monoclinic (JCPDS No. 83–1462) and hexagonal Cu_2S (JCPDS No. 84–0206), and cubic Co_3S_4 phases (JCPDS No. 47–1738),

[a] College of Chemistry, Sichuan University, Chengdu 610064, Sichuan, China. E-mail: sunxp@scu.edu.cn, sunxp_scu@hotmail.com
[b] College of Chemistry and Chemical Engineering, Qufu Normal University, Qufu 273165, Shandong, China
[c] Chengdu Institute of Geology and Mineral Resources, Chengdu 610081, Sichuan, China
[d] Chemistry Department, Faculty of Science, King Abdulaziz University, Jeddah 21589, Saudi Arabia
[e] College of Materials Science and Engineering, Sichuan University, Chengdu 610064, Sichuan, China

† Electronic supplementary information (ESI) available: Experimental section and supplementary figures. See DOI: 10.1039/c7cc07259g

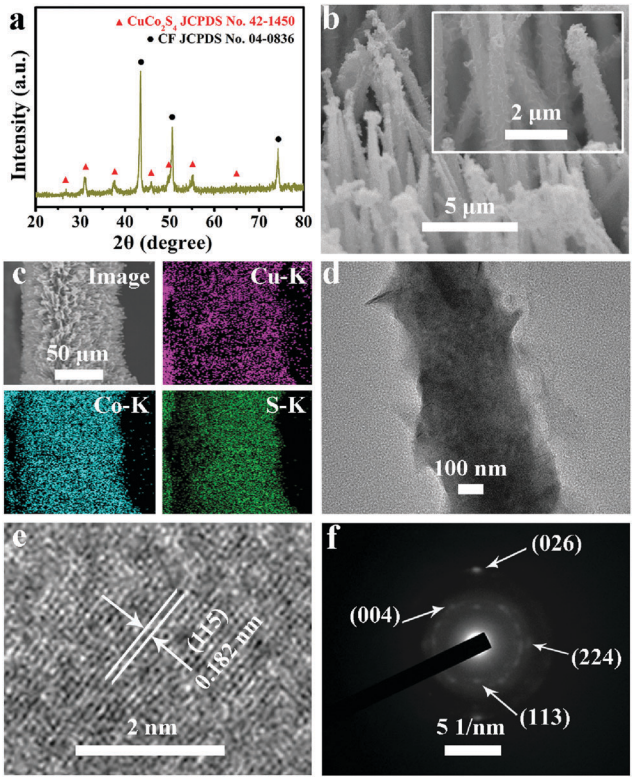

Fig. 1 (a) XRD pattern for $CuCo_2S_4$/CF. (b) SEM images for $CuCo_2S_4$/CF. (c) SEM image and EDX elemental mapping images for Cu, Co, and S elements in $CuCo_2S_4$/CF. (d) TEM and (e) HRTEM images for $CuCo_2S_4$. (f) SAED patterns for $CuCo_2S_4$.

respectively. The scanning electron microscopy (SEM) images of the hydroxide precursor indicate that it is a nanowire array (Fig. S2, ESI†). After a hydrothermal sulfidization process, the as-prepared $CuCo_2S_4$ still preserves the 1D morphology but with many ultrathin nanosheets on the surface, suggesting the formation of the hierarchical structure (Fig. 1b). The low-magnification SEM image in Fig. 1c indicates that the $CuCo_2S_4$ is well aligned on the CF substrate, and the corresponding energy-dispersive X-ray (EDX) elemental mapping images verify the uniform distribution of Cu, Co, and S elements. Cu–S/CF, Co–S/CF, and CuCo–S with varied Co^{2+}/Cu^{2+} ratios were also prepared for comparison (Fig. S2, S3, and S4, ESI†). Fig. S5 (ESI†) shows the EDX spectrum of $CuCo_2S_4$/CF, further showing the existence of Cu, Co, and S elements with an atomic ratio close to 1 : 2 : 4. The high-resolution transmission electron microscopy (HRTEM) analysis (Fig. 1e) taken from $CuCo_2S_4$ (Fig. 1d) reveals lattice fringes with an interplanar distance of 0.182 nm indexed to the (115) plane of the cubic $CuCo_2S_4$ phase. The selected area electron diffraction (SAED) pattern shows discrete spots of the (113), (004), (224), and (026) planes of crystalline cubic $CuCo_2S_4$ (Fig. 1f).

The X-ray photoelectron spectroscopy (XPS) survey spectrum for $CuCo_2S_4$/CF (Fig. 2a) confirms the presence of Cu, Co, and S elements. The binding energies (BEs) at 952.3 and 932.5 eV in the Cu 2p region (Fig. 2b) can be assigned to Cu $2p_{1/2}$ and Cu $2p_{3/2}$, respectively, indicating the presence of Cu^{+}.[53,54] The other two shakeup satellite peaks (identified as Sat.) at 954.0 and 934.5 eV,

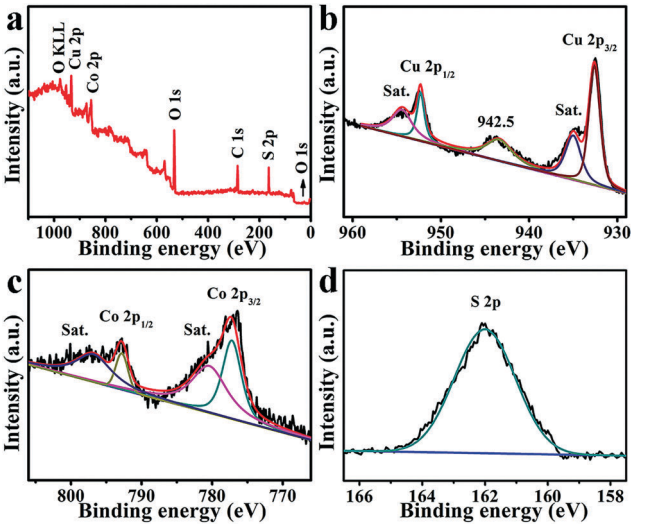

Fig. 2 (a) XPS survey spectrum for $CuCo_2S_4$. XPS spectra for $CuCo_2S_4$ in the (b) Cu 2p, (c) Co 2p, and (d) S 2p regions.

together with the peak at 942.5 eV, suggest the existence of Cu^{2+} arising from air exposure.[52,55] In the Co 2p region (Fig. 2c), the BEs of Co $2p_{1/2}$ and Co $2p_{3/2}$ appear at 792.8 and 778.0 eV, respectively, with two shakeup satellites at 796.8 and 780.8 eV, indicating the coexistence of Co^{2+} and Co^{3+}.[53,54] The BE at 162.0 eV in the S 1s region (Fig. 2c) is assigned to the Cu–S and Co–S bonds, and low coordination of S^{2-} at the surface.[52,53]

We collected the linear sweep voltammetry (LSV) curves to evaluate the electrocatalytic activity of $CuCo_2S_4$/CF ($CuCo_2S_4$ loading: 3.6 mg cm^{-2}) toward water oxidation on a typical three-electrode setup with a scan rate of 5 mV s^{-1} in 1.0 M KOH. For comparison, Cu–S/CF, Co–S/CF, RuO_2 (Fig. S6, see ESI† for preparation details) on CF (RuO_2/CF, with the same mass loading), and bare CF were also investigated under the same conditions. Owing to the solution resistance, all experimental data were corrected with ohmic potential drop (iR) losses to reflect the intrinsic behavior of the catalysts, and all potentials were reported on a reversible hydrogen electrode (RHE) scale except specifically stated. Fig. 3a shows the LSV curves. As observed, RuO_2/CF exhibits high activity for water oxidation with the need of a low overpotential of 276 mV to achieve 100 mA cm^{-2}, whereas the bare CF shows poor catalytic activity. Cu–S/CF is also active for water oxidation, requiring overpotential of 472 mV to afford 100 mA cm^{-2}. Although Co–S/CF shows better catalytic activity for water oxidation, it still needs an overpotential of 340 mV to drive the same current density. Impressively, our $CuCo_2S_4$/CF is superior in catalytic activity, demanding an overpotential of only 295 mV to deliver 100 mA cm^{-2}, 177 and 45 mV less than those of monometallic Cu–S/CF and Co–S/CF, respectively. The oxidative feature at 1.35 and 1.47 V (as marked by the blue dash lines) preceding water oxidation is the oxidation of the $CuCo_2S_4$/CF catalyst.[51] Additionally, it needs a much smaller overpotential of 259 mV to afford the geometric current density of 60 mA cm^{-2}, comparing favorably to the behaviors of most reported non-noble metal WOCs at alkaline pH, like Al–CoP/NF (η_{50} mA cm^{-2} = 280 mV),[56] $MnCo_2S_4$ NA/TM (η_{50} mA cm^{-2} = 325 mV),[38] $NiCo_2S_4$ NA/CC

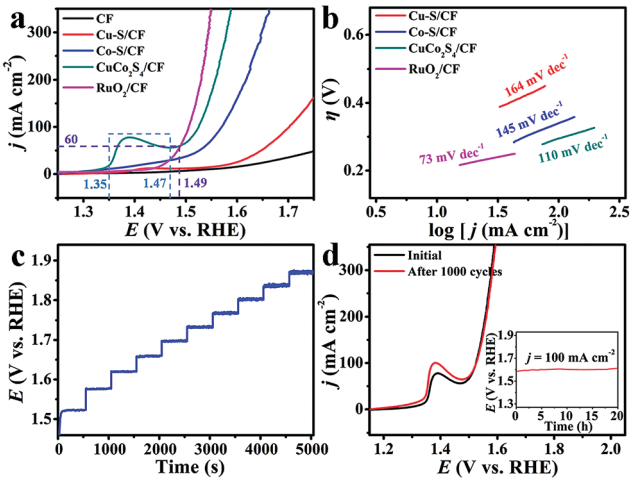

Fig. 3 (a) LSV curves of RuO_2/CF, $CuCo_2S_4$/CF, Cu–S/CF, Co–S/CF, and bare CF with a scan rate of 5 mV s^{-1} for water oxidation. (b) Tafel plots for RuO_2/CF, $CuCo_2S_4$/CF, Co–S/CF, and Cu–S/CF. (c) Multi-current process for $CuCo_2S_4$/CF. The current density started at 40 mA cm^{-2} and ended at 400 mA cm^{-2}, with an increment of 40 mA cm^{-2} per 500 s without iR correction. (d) LSV curves for $CuCo_2S_4$/CF before and after 1000 cyclic voltammetry cycles (inset: chronopotentiometric curve for $CuCo_2S_4$/CF at a constant current density of 100 mA cm^{-2} without iR correction). All experiments were performed in 1.0 M KOH unless specially stated.

(η_{100} mA cm^{-2} = 340 mV),[34] $NiSe_2$/Ti (η_{20} mA cm^{-2} = 295 mV),[57] De-LNiFeP/rGO (η_{10} mA cm^{-2} = 258 mV),[12] *etc.*, and a detailed comparison is listed in Table S1 (ESI†). Fig. 3b presents the Tafel plots of Cu–S/CF, Co–S/CF, $CuCo_2S_4$/CF, and RuO_2/CF. The Tafel slope of 110 mV dec^{-1} for $CuCo_2S_4$/CF is much smaller than those for Cu–S/CF (164 mV dec^{-1}) and Co–S/CF (145 mV dec^{-1}), implying a more favorable catalytic kinetics on $CuCo_2S_4$/CF. We also examined the effect of the Co^{2+}/Cu^{2+} ratio on the water oxidation activity, and overpotentials of 450, 416, 352, and 311 mV are needed to drive a geometric current density of 100 mA cm^{-2} for Cu_3Co–S/CF, Cu_2Co–S/CF, CuCo–S/CF, and $CuCo_3$–S/CF, respectively (Fig. S7, ESI†).

Fig. 3c displays the multi-step chronopotentiometric curve for $CuCo_2S_4$/CF. The anodic current density increases from 40 to 400 mA cm^{-2} with an increment of 40 mA cm^{-2} per 500 s, and the potential immediately levels off at 1.52 V for the starting current value, remaining constant for the rest 500 s. Similar results are observed for other steps tested up to 400 mA cm^{-2}, demonstrating the excellent mass transport properties, conductivity, and mechanical robustness of the $CuCo_2S_4$/CF electrode.[13,58] Given that stability is also a critical criterion for the practical applications of catalysts, we thus probed the stability of our $CuCo_2S_4$/CF *via* continuous cyclic voltammetry scanning. The LSV curve shows negligible loss in current density after 1000 cycles compared with the initial one (Fig. 3d), suggesting its superior stability. An electrolysis measurement at a fixed current density of 100 mA cm^{-2} further demonstrates that this catalyst has strong long-term electrochemical durability, maintaining its catalytic activity for at least 20 h (Fig. 3d, inset). $CuCo_2S_4$/CF still retains its hierarchical feature after the stability test (Fig. S8, ESI†). The XRD pattern also shows characteristic peaks of cubic $CuCo_2S_4$ but with decreased intensities (Fig. S9, ESI†). A thin amorphous layer about 2–3 nm was formed on the $CuCo_2S_4$ surface (Fig. S10, ESI†). We also performed XPS analysis of the sample after oxidation electrolysis. In the Cu 2p region (Fig. S11a, ESI†), the BEs at 934.5 ($2p_{1/2}$) and 954.6 eV ($2p_{3/2}$), together with the peaks at 939.5 and 941.7 eV, suggest the existence of CuO.[59] The BE at 962.8 eV indicates the presence of $Cu(OH)_2$.[60] In the Co 2p region (Fig. S11b, ESI†), the strong peak at 780.4 eV ($2p_{3/2}$) can be assigned to CoO.[61] The peaks at 782.3 (Sat.), 795.4 ($2p_{1/2}$), and 796.8 eV arise from $Co(OH)_2$.[34,62] Another wide peak appearing at 787.0 eV implies the presence of CoOOH.[63] The peak for S^{2-} in the S 2p region can hardly be observed (Fig. S11c). In the O 1s region (Fig. S11d, ESI†), the BE at 529.3 eV and a weak peak at 531.3 eV suggest the existence of O^{2-} and OH^- species, respectively.[64] These observations suggest the formation of an amorphous oxide/(oxy)hydroxide layer on the $CuCo_2S_4$ surface as the real active phase.[34]

To estimate the electrochemically active surface area, we determined the electrochemical double-layer capacitance (C_{DL}) at the solid/liquid interface for Cu–S/CF, Co–S/CF, $CuCo_2S_4$/CF from cyclic voltammograms (CVs).[65,66] All CVs were collected in the region of 0.608–0.708 V (Fig. S9a–c, ESI†) to ensure that the current responses are only owing to the charging of the double layer. According to the formula: $j_c = \nu C_{DL}$ (a plot of j_c as a function of ν yields a straight line with a slope equal to C_{DL}), the C_{DL} values for Cu–S/CF, Co–S/CF, and $CuCo_2S_4$/CF are 1.990, 2.390, and 3.300 mF cm^{-2}, respectively (Fig. S9d, ESI†), implying $CuCo_2S_4$/CF has a much larger surface area and more exposed active sites.[6]

To calculate TOF, we applied electrochemistry to quantify the surface concentration of active sites (Fig. 4a).[67] We assumed a one-electron oxidation process for the oxidation of Cu and Co metal centers in $CuCo_2S_4$.[38] There exists a linear dependence between the oxidation peak current density for redox Cu and Co species and scan rates (Fig. 4a, inset). The TOF values for $CuCo_2S_4$/CF are calculated to be 0.069 and 0.390 mol O_2 s^{-1} at overpotentials of 300 and 400 mV, respectively (Fig. 4b), much higher than those for reported WOCs like $MnCo_2S_4$ NA/TM (~0.20 mol O_2 s^{-1}, η = 400 mV),[38] Co_3O_4/N–PC (0.0015 mol O_2 s^{-1}, η = 300 mV),[68] and $NiCo_2O_4$@Ni–Co–B/CC (0.019 mol O_2 s^{-1}, η = 300 mV).[69]

In summary, a hierarchical $CuCo_2S_4$ nanoarray has been developed for durable water oxidation electrolysis with the need of overpotential of 295 mV to afford a geometrical catalytic current density of 100 mA cm^{-2} in 1.0 M KOH. It also achieves high TOF of 0.069 and 0.390 mol O_2 s^{-1} at overpotentials of 300 and 400 mV, respectively. This nanoarray may hold great

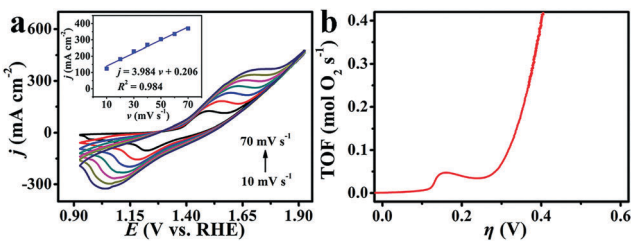

Fig. 4 (a) CVs for $CuCo_2S_4$/CF in the faradic capacitance current range at scan rates from 10 to 70 mV s^{-1} (inset: the corresponding plot of oxidation peak current density *versus* the scan rate from CVs) in 1.0 M KOH. (b) A plot of TOF for $CuCo_2S_4$/CF as a function of overpotential.

promise as an attractive water-oxidizing catalyst material in water-splitting devices toward large-scale production of hydrogen fuels for applications.

This work was supported by the National Natural Science Foundation of China (No. 21575137).

Conflicts of interest

There are no conflicts to declare.

References

1 J. Chow, R. J. Kopp and P. R. Portney, *Science*, 2003, **302**, 1528–1531.
2 T. R. Cook, D. K. Dogutan, S. Y. Reece, Y. Surendranath, T. S. Teets and D. G. Nocera, *Chem. Rev.*, 2010, **110**, 6474–6502.
3 D. G. Nocera, *Acc. Chem. Res.*, 2012, **45**, 767–776.
4 M. S. Dresselhaus and I. L. Thomas, *Nature*, 2001, **414**, 332–337.
5 W. Hong, M. Risch, K. A. Stoerzinger, A. Grimaud, J. Suntivich and Y. Shao-Horn, *Energy Environ. Sci.*, 2015, **8**, 1404–1427.
6 W. Zhu, R. Zhang, F. Qu, A. M. Asiri and X. Sun, *ChemCatChem*, 2017, **9**, 1721–1743.
7 Q. Yin, J. M. Tan, C. Besson, Y. V. Geletii, D. G. Musaev, A. E. Kuznetsov, Z. Luo, K. I. Hardcastle and C. L. Hill, *Science*, 2010, **328**, 342–345.
8 J. Suntivich, K. J. May, H. A. Gasteiger, J. B. Goodenough and Y. Shao-Horn, *Science*, 2011, **334**, 1383–1385.
9 J. Wang, X. Ma, F. Qu, A. M. Asiri and X. Sun, *Inorg. Chem.*, 2017, **56**, 1041–1044.
10 Y. Lee, J. Suntivich, K. J. May, E. E. Perry and Y. Shao-Horn, *J. Phys. Chem. Lett.*, 2012, **3**, 399–404.
11 X. Ji, S. Hao, F. Qu, J. Liu, G. Du, A. M. Asiri, L. Chen and X. Sun, *Nanoscale*, 2017, **9**, 7714–7718.
12 Y. Liu, H. Wang, D. Lin, C. Liu, P. C. Hsu, W. Liu, W. Chen and Y. Cui, *Energy Environ. Sci.*, 2015, **8**, 1719–1724.
13 W. Lu, T. Liu, L. Xie, C. Tang, D. Liu, S. Hao, F. Qu, G. Du, Y. Ma, A. M. Asiri and X. Sun, *Small*, 2017, **13**, 1700805.
14 M. Gao, Y. Xu, J. Jian, Y. Zheng and S. Yu, *J. Am. Chem. Soc.*, 2012, **134**, 2930–2933.
15 Z. Zhao, H. Wu, H. He, X. Xu and Y. Jin, *Adv. Funct. Mater.*, 2014, **24**, 4698–4705.
16 H. Liang, F. Meng, M. Caban–Acevedo, L. Li, A. Forticaux, L. Xiu, Z. Wang and S. Jin, *Nano Lett.*, 2015, **15**, 1421–1427.
17 X. Lu, L. Gu, J. Wang, J. Wu, P. Liao and G. Li, *Adv. Mater.*, 2017, **29**, 1604437.
18 B. Weng, F. Xu, C. Wang, W. Meng, C. R. Grice and Y. Yan, *Energy Environ. Sci.*, 2017, **10**, 121–128.
19 S. Dou, C. Dong, Z. Hu, Y. Huang, J. Chen, L. Tao, D. Yan, D. Chen, S. Shen, S. Chou and S. Wang, *Adv. Funct. Mater.*, 2017, **27**, 1702546.
20 M. B. Stevens, L. J. Enman, A. S. Batchellor, M. R. Cosby, A. E. Vise, C. D. M. Trang and S. W. Boettcher, *Chem. Mater.*, 2017, **29**, 120–140.
21 C. Hu, L. Zhang, Z. Zhao, J. Luo, J. Shi, Z. Huang and J. Gong, *Adv. Mater.*, 2017, **29**, 1701820.
22 I. A. Moreno-Hernandez, C. A. MacFarland, C. G. Read, B. S. Brunschwig, K. M. Papadantonakis and N. Lewis, *Energy Environ. Sci.*, 2017, **10**, 2103–2108.
23 L. Ji, Z. Lin, M. Alcoutlabi and X. Zhang, *Energy Environ. Sci.*, 2011, **4**, 2682–2699.
24 X. Xu, W. Liu, Y. Kim and J. Cho, *Nano Today*, 2014, **9**, 604–630.
25 Q. Chen, F. Lu, Y. Xia, H. Wang and X. Kuang, *J. Mater. Chem. A*, 2017, **5**, 4075–4083.
26 M. Yan, Y. Yao, J. Wen, L. Long, M. Kong, G. Zhang, X. Liao, G. Yin and Z. Huang, *ACS Appl. Mater. Interfaces*, 2016, **8**, 24525–24535.
27 Z. Xing, Q. Chu, X. Ren, C. Ge, A. H. Qusti, A. M. Asiri, A. O. Al-Youbi and X. Sun, *J. Power Sources*, 2014, **245**, 463–467.
28 P. Zhang, B. Y. Guan, L. Yu and X. W. Lou, *Angew. Chem., Int. Ed.*, 2017, **56**, 7141–7145.
29 H. Li, J. Liu, J. Li, Y. Hu, W. Wang, D. Yuan, Y. Wang, T. Yang, L. Li, H. Sun, S. Ren, X. Zhu, Q. Guo, X. Wen, Y. Li and B. Shen, *ACS Catal.*, 2017, **7**, 4805–4816.
30 O. Y. Gutiérrez, S. Singh, E. Schachtl, J. Kim, E. J. Hein and J. A. Lercher, *ACS Catal.*, 2014, **4**, 1487–1499.
31 W. Lai, Z. Chen, J. Zhu, L. Yang, J. Zheng, X. Yi and W. Fang, *Nanoscale*, 2016, **8**, 3823–3833.
32 X. Ren, W. Wang, R. Ge, S. Hao, F. Qu, G. Du, A. M. Asiri, Q. Wei, L. Chen and X. Sun, *Chem. Commun.*, 2017, **53**, 9000–9003.
33 Q. Li, Z. Xing, D. Wang, X. Sun and X. Yang, *ACS Catal.*, 2016, **6**, 2797–2801.
34 D. Liu, Q. Lu, Y. Luo, X. Sun and A. M. Asiri, *Nanoscale*, 2015, **7**, 15122–15126.
35 N. Yang, C. Tang, K. Wang, G. Du, A. M. Asiri and X. Sun, *Nano Res.*, 2016, **9**, 3346–3354.
36 Z. Xing, X. Yang, A. M. Asiri and X. Sun, *ACS Appl. Mater. Interfaces*, 2016, **8**, 14521–14526.
37 W. Wang, L. Yang, F. Qu, Z. Liu, G. Du, A. M. Asiri, Y. Yao, L. Chen and X. Sun, *J. Mater. Chem. A*, 2017, **5**, 16585–16589.
38 X. Zhang, C. Si, X. Guo, R. Kong and F. Qu, *J. Mater. Chem. A*, 2017, **5**, 17211–17215.
39 P. Chen, T. Zhou, M. Zhang, Y. Tong, C. Zhong, N. Zhang, L. Zhang, C. Wu and Y. Xie, *Adv. Mater.*, 2017, **29**, 1701584.
40 J. Liu, J. Wang, B. Zhang, Y. Ruan, L. Lv, X. Ji, K. Xu, L. Miao and J. Jiang, *ACS Appl. Mater. Interfaces*, 2017, **9**, 15364–15372.
41 W. Fang, D. Liu, Q. Lu, X. Sun and A. M. Asiri, *Electrochem. Commun.*, 2016, **63**, 60–64.
42 N. Cheng, Q. Liu, A. M. Asiri, W. Xing and X. Sun, *J. Mater. Chem. A*, 2015, **3**, 23207–23212.
43 T. Liu, X. Sun, A. M. Asiri and Y. He, *Int. J. Hydrogen Energy*, 2016, **41**, 7264–7269.
44 L. Mei, T. Yang, C. Xu, M. Zhang, L. Chen, Q. Li and T. Wang, *Nano Energy*, 2014, **3**, 36–45.
45 L. Shen, J. Wang, G. Xu, H. Li, H. Dou and X. Zhang, *Adv. Energy Mater.*, 2015, **5**, 1400977.
46 A. M. Elshahawy, X. Li, H. Zhang, Y. Hu, K. H. Ho, C. Guan and J. Wang, *J. Mater. Chem. A*, 2017, **5**, 7494–7506.
47 Z. Pu, Q. Liu, P. Jiang, A. M. Asiri, A. Y. Obaid and X. Sun, *Chem. Mater.*, 2014, **26**, 4326–4329.
48 L. Xie, C. Tang, K. Wang, G. Du, A. M. Asiri and X. Sun, *Small*, 2017, **13**, 1602755.
49 Z. Li, M. Shao, L. Zhou, R. Zhang, C. Zhang, J. Han, M. Wei, D. G. Evans and X. Duan, *Nano Energy*, 2016, **20**, 294–304.
50 Q. Yang, T. Li, Z. Lu, X. Sun and J. Liu, *Nanoscale*, 2014, **6**, 11789–11794.
51 X. Liu, Z. Chang, L. Luo, T. Xu, X. Lei, J. Liu and X. Sun, *Chem. Mater.*, 2014, **26**, 1889–1895.
52 J. Tang, Y. Ge, J. Shen and M. Ye, *Chem. Commun.*, 2016, **52**, 1509–1512.
53 S. E. Moosavifard, S. Fani and M. Rahmanian, *Chem. Commun.*, 2016, **52**, 4517–4520.
54 B. Li, F. Yuan, G. He, X. Han, X. Wang, J. Qin, Z. Guo, X. Lu, Q. Wang, I. P. Parkin and C. Wu, *Adv. Funct. Mater.*, 2017, **27**, 1606218.
55 M. Zhang, K. P. Annamalai, L. Liu, T. Chen, J. Gao and Y. Tao, *RSC Adv.*, 2017, **7**, 20724–20731.
56 R. Zhang, C. Tang, R. Kong, G. Du, A. M. Asiri, L. Chen and X. Sun, *Nanoscale*, 2017, **9**, 4793–4800.
57 Z. Pu, Y. Luo, A. M. Asiri and X. Sun, *ACS Appl. Mater. Interfaces*, 2016, **8**, 4718–4723.
58 F. Xie, H. Wu, J. Mou, D. Lin, C. Xu, C. Wu and X. Sun, *J. Catal.*, 2017, **356**, 165–172.
59 L. Cui, X. Cao, X. Sun, W. Yang and J. Liu, *ChemCatChem*, DOI: 10.1002/cctc.201701317.
60 J. Yu and J. Ran, *Energy Environ. Sci.*, 2011, **4**, 1364–1371.
61 T. J. Chuang, C. R. Bidle and D. W. Rice, *Surf. Sci.*, 1976, **59**, 413–429.
62 C. Mondal, M. Ganguly, P. K. Manna, S. M. Yusuf and T. Pal, *Langmuir*, 2013, **29**, 9179–9187.
63 J. Yang and T. Sasaki, *Chem. Mater.*, 2008, **20**, 2049–2056.
64 R. Zhang, Z. Wang, S. Hao, R. Ge, X. Ren, F. Qu, G. Du, A. M. Asiri, B. Zheng and X. Sun, *ACS Sustainable Chem. Eng.*, 2017, **5**, 8518–8522.
65 C. C. L. McCrory, S. Jung, J. C. Peters and T. F. Jaramillo, *J. Am. Chem. Soc.*, 2013, **135**, 16977–16987.
66 J. D. Benck, Z. Chen, L. Y. Kuritzky, A. J. Forman and T. F. Jaramillo, *ACS Catal.*, 2012, **2**, 1916–1923.
67 M. Xie, L. Yang, Y. Ji, Z. Wang, X. Ren, Z. Liu, A. M. Asiri, X. Xiong and X. Sun, *Nanoscale*, 2017, **9**, 16612–16615.
68 Y. Hou, J. Li, Z. Wen, S. Cui, C. Yuan and J. Chen, *Nano Energy*, 2015, **12**, 1–8.
69 X. Ji, X. Ren, S. Hao, F. Xie, F. Qu, G. Du, A. M. Asiri and X. Sun, *Inorg. Chem. Front.*, 2017, **4**, 1546–1550.